



## Search for electron capture in $^{176}\text{Lu}$ with a lutetium yttrium oxyorthosilicate scintillator

Luigi Ernesto Ghezzer, Francesco Nozzoli <sup>\*</sup>, Riccardo Nicolaidis, Roberto Iuppa, and Paolo Zuccon   
*INFN-TIFPA and Department of Physics, Trento University, Via Sommarive 14 I-38123 Trento, Italy*

Cristian De Santis 

*INFN-Sezione di Roma Tor Vergata, Via della Ricerca Scientifica 1, I-00133 Rome, Italy*



(Received 29 November 2022; accepted 3 April 2023; published 28 April 2023)

The nuclide  $^{176}\text{Lu}$  is one of the few naturally occurring isotopes that are potentially unstable with respect to electron capture (EC). Although experimental evidence for  $^{176}\text{Lu}$  EC decay is still missing, this isotope is instead well known to  $\beta^-$  decay into  $^{176}\text{Hf}$  with a half-life of about 38 Gyr. The precise investigation of all possible decay modes for  $^{176}\text{Lu}$  is interesting because the Lu/Hf ratio is adopted as an isotopic clock. Previous searches for the  $^{176}\text{Lu}$  EC decay were performed by using a passive lutetium source coupled with a high-purity germanium (HPGe) spectrometer. Our approach uses a lutetium yttrium oxyorthosilicate (LYSO) crystal both as a lutetium source and as an active detector. Scintillation light from the LYSO crystal is acquired together with the signals from the HPGe detector, and this allows a powerful suppression of the background sourcing from the well-known  $\beta^-$ -decay branch. This approach led to an improvement on the  $^{176}\text{Lu}$  EC branching ratio limits by a factor of 3 to 30, depending on the considered EC channel.

DOI: [10.1103/PhysRevC.107.045504](https://doi.org/10.1103/PhysRevC.107.045504)

### I. INTRODUCTION

The naturally occurring isotope  $^{176}\text{Lu}$  (2.6% abundance) is known to  $\beta^-$  decay to  $^{176}\text{Hf}$  with a half-life of  $\approx 38$  Gyr. However,  $^{176}\text{Lu}$  is also one of the six naturally occurring isotopes that are potentially unstable with respect to electron capture (EC). In particular, evidence for EC decay has been found for  $^{40}\text{K}$  [1],  $^{50}\text{V}$  [2,3], and  $^{138}\text{La}$  [1], but is still missing for  $^{123}\text{Te}$  [4],  $^{176}\text{Lu}$  [5], and  $^{180m}\text{Ta}$  [6]. The precise investigation of all possible radioactive decay modes of  $^{176}\text{Lu}$  is interesting because the Lu/Hf ratio is an isotopic clock to date meteorites and minerals. In particular, it has been suggested that some discrepancies involving Lu/Hf age comparisons in different samples could be reconciled if  $^{176}\text{Lu}$  also underwent significant EC decay [5,7,8]. A second interesting feature is that  $^{176}\text{Lu}/^{175}\text{Lu}$  can be considered also as an s-process thermometer in studies of stellar nucleosynthesis [9].

Figure 1 shows the decay scheme of  $^{176}\text{Lu}$ : on the right side the dominant decay chain to  $^{176}\text{Hf}$  is depicted, while on the left side there is the expected EC decay process to  $^{176}\text{Yb}$ . The  $Q$  value for EC decay of  $^{176}\text{Lu}$  ( $J^\pi = 7^-$ ) to the  $^{176}\text{Yb}$  ground state ( $J^\pi = 0^+$ ) is  $\approx 109$  keV [11–13], and the one to the  $^{176}\text{Yb}$  first excited state ( $J^\pi = 2^+$ ) is  $\approx 27$  keV. These EC decay branches, however, would be forbidden transitions of the seventh and fifth order, respectively. The relative branching ratios are then expected to be very small, also considering that forbidden transitions of orders greater than the fourth order have never been experimentally observed so far [14].

Previous searches for the  $^{176}\text{Lu}$  EC decay were performed by using a passive lutetium source coupled to a high-purity

germanium (HPGe) detector used to search for the  $^{176}\text{Yb}^*$  82-keV  $\gamma$  ray or the characteristic Yb x rays [5]. Our approach, which we call “active source,” uses a lutetium yttrium oxyorthosilicate (LYSO) [15] crystal scintillator coupled to a photomultiplier tube (PMT) both as a  $^{176}\text{Lu}$  source and as a detector. The LYSO crystal PMT signal was acquired together with the signal from an HPGe detector, this allows a powerful reduction of the large background from the  $\beta^-$ -decay branch. Moreover the possibility of a simultaneous measurement of the energy release within the LYSO crystal allows also the investigation of the different EC decay channels.

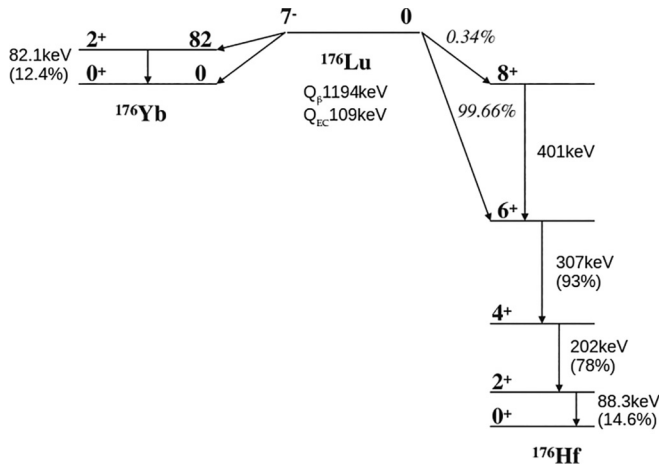
In these cases of highly forbidden transitions, which are suppressed by a large variation of the nucleus spin as compared with the sum of the angular momentum of the captured electron and of the emitted neutrino, an important channel for the decay is provided by the radiative electron capture (REC) [16]. In this process an x ray can be radiated either by the captured electron (internal bremsstrahlung) or by the father or daughter nucleus (detour transitions); this photon contributes with its spin to the overall angular momentum conservation. The REC decay has been experimentally observed for the forbidden decay of  $^{41}\text{Ca}$ ,  $^{59}\text{Ni}$ ,  $^{81}\text{Kr}$ ,  $^{137}\text{La}$ , and  $^{204}\text{Tl}$  [17–21].

In our setup the energy released by an occurring REC x ray, combined with the energy released by the atomic relaxation of the electron vacancy, would be measured by the LYSO scintillator. This measurement, when combined with the signals from the HPGe detector, boosts the capability to identify the  $^{176}\text{Lu}$  EC decays.

### II. EXPERIMENTAL SETUP

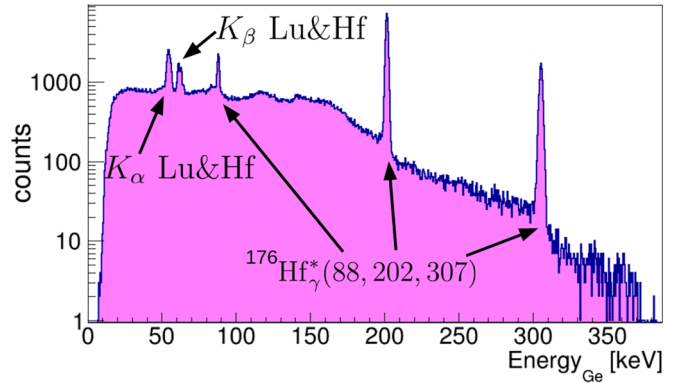
The measurements were performed using the HPGe facility at the physics department of the Trento University; a flat sliced

<sup>\*</sup>Francesco.Nozzoli@cern.ch


 FIG. 1. Decay scheme of  $^{176}\text{Lu}$  [10,11].

LYSO crystal (elliptical shape of size  $\approx 35 \times 20 \times 2$  mm<sup>3</sup>, 7.9 g) was coupled to a Hamamatsu-R5946 ( $\varnothing 38$  mm) PMT with an EJ-550 optical couplant. The expected LYSO source activity is  $\approx 40$  Bq/g due to the known  $^{176}\text{Lu}$   $\beta$  decay. This active LYSO source was placed in front of a CANBERRA GC2020 HPGe [22] and the two detectors were shielded with 2.5 mm of Cu and 5 cm of Pb to minimize the environmental  $\gamma$  background. The inner Cu shield is meant to stop the 84.9-keV Pb  $K_{\beta}$  x rays that are produced by the external Pb shield and that would provide a background near to the 82.1-keV  $^{176}\text{Yb}^*$  signal region. Both detector signals were digitized by a LeCroy HDO9104 [23] in a 20- $\mu\text{s}$ -wide time window, and the acquisition trigger was set on the HPGe signal with an energy threshold of  $\approx 15$  keV. No trigger conditions were imposed on the LYSO signals, because this allowed us to study all the possible EC channels, like the previous experiments using the passive  $^{176}\text{Lu}$  source. A total number of  $1.5 \times 10^6$  events were acquired during the 90-h exposure time. LYSO is a good scintillating material ( $\approx 33$  ph/keV) with a fast ( $\approx 40$  ns) decay time, and despite the signal of HPGe being much slower, we achieved a coincidence time resolution of  $\approx 100$  ns in our measurements. Energy calibration of the HPGe detector was done using the characteristic  $\gamma$  lines produced by  $^{176}\text{Lu}$   $\beta$  decay in  $^{176}\text{Hf}^*$  excited levels. Figure 2 shows the energy spectrum measured by our HPGe detector.

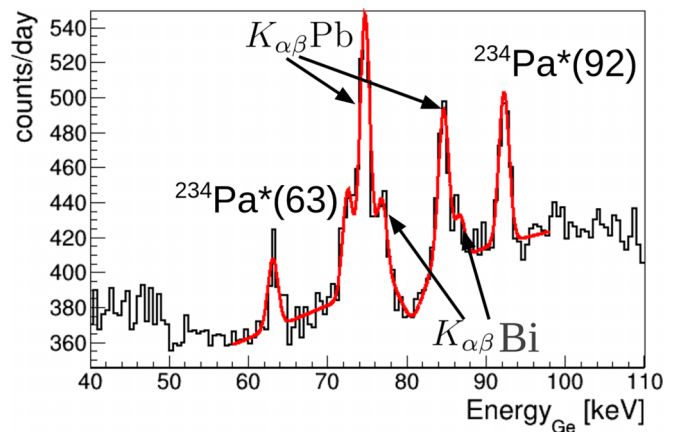
The HPGe detector shows an energy resolution of  $1.50 \pm 0.05$  keV FWHM at 88 keV, and  $1.65 \pm 0.10$  keV FWHM at 55 keV. A measurement of the background for the whole experiment was performed by removing only the thin LYSO crystal from the setup; the HPGe energy spectrum acquired during a 90-h exposure time is shown in Fig. 3. Around 82 keV in the region of interest for the  $^{176}\text{Lu}$  EC, it is possible to identify the residual Pb x rays: 84.9-keV  $K_{\beta}$ , 75-keV  $K_{\alpha 1}$ , and 72.8-keV  $K_{\alpha 2}$  surviving the inner Cu shield. In addition to Pb x-rays, also the characteristic  $\gamma$  lines of  $^{234}\text{Pa}^*$  are identified in the background; they occur in common materials, with  $^{234}\text{Pa}$  being a daughter isotope in the  $^{238}\text{U}$  natural radioactive chain [24]. Also, a hint for the possible contribution of Bi x rays to the intrinsic background is observable. In particular  $^{214}\text{Bi}$  and  $^{210}\text{Bi}$  belong to the


 FIG. 2. HPGe energy spectrum measured in  $\approx 90$ -h exposure.

$^{238}\text{U}$  natural radioactive chain, whereas  $^{212}\text{Bi}$  belongs to the  $^{232}\text{Th}$  one.

The large density and the effective atomic number (7.1 g/cm<sup>3</sup>,  $Z_{\text{eff}} = 65$ ) provide a good  $\gamma$ -ray detection capability for the LYSO scintillator, and at the same time, this puts a limit on the probability of the  $\gamma$  ray to escape the crystal and reach the HPGe detector. This dictates the thin slice geometry we chose for our LYSO crystal. The overall  $\gamma$ -ray detection efficiency can be estimated by comparing the measured HPGe spectra with the known intensity ratios of  $K_{\beta 1,2,3}/K_{\alpha 1,2}$  lines in Lu and Hf and with the amplitude of  $^{176}\text{Hf}^*$   $\gamma$  lines once the internal conversion coefficients are taken into account [1,10,25].

The measured detection efficiency,  $\varepsilon_{88}$ , relative to the efficiency for detection of  $\gamma$  rays with 88-keV energy, is shown in Fig. 4. The efficiency behavior is dominated, at low energy, by the photoelectric cross section on lutetium. It is interesting to note that Hf  $K_{\beta 2}$  x rays (65 keV) are just above the 63.3-keV Lu  $k$ -edge, whereas Hf  $K_{\beta 1,3}$  x rays (63.2 and 63 keV) are just below. The red line in Fig. 4 shows the expected  $\varepsilon_{88}$  behavior considering the self-absorption of 2-mm-thick LYSO crystal [15] combined with the efficiency of the GC2020 HPGe detector [22]. The efficiency for  $^{176}\text{Yb}^*$  82.1 keV is  $\approx 80\%$  with


 FIG. 3. Intrinsic and environmental HPGe background spectra. The red line is a background model, as a guide to the eye, whereas the  $\gamma$  lines of  $^{234}\text{Pa}^*$  and the x rays from Pb and Bi are identified.

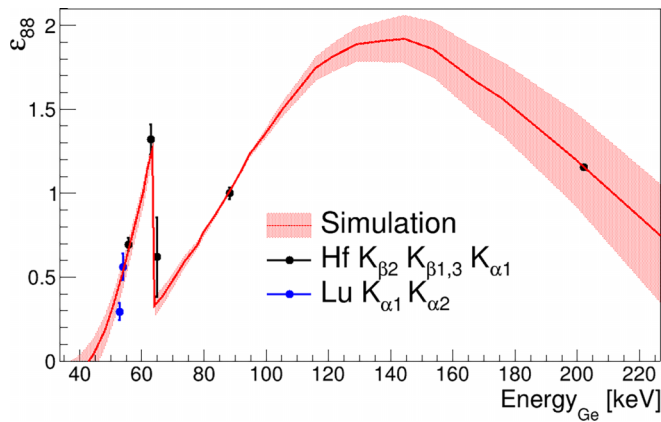


FIG. 4. HPGe detection efficiency,  $\varepsilon_{88}$ , (relative to 88 keV) for  $\gamma$  and x rays emitted by the LYSO active source. The red line shows the expected behavior considering the self-absorption of the LYSO crystal [15] combined with the efficiency of the GC2020 HP-Ge detector [22].

respect to that of 88 keV, whereas the efficiency for Yb  $K_{\beta}$  (59.3 keV) is almost the same.

The calibration of the LYSO scintillator was performed with  $^{241}\text{Am}$  and  $^{137}\text{Cs}$  external sources. Figure 5 shows the collected energy spectrum using  $^{241}\text{Am}$ ; beyond the known 59.5-keV peak from the  $^{237}\text{Np}^*$  decay, it is also possible to observe, at lower energy, the folded contribution of 13.9-17.8-20.8 keV due to  $L_{\alpha\beta\gamma}$  Np x rays.

LYSO scintillators are affected by a nonproportionality for the  $\gamma$ -ray response at low energy [26–28]. Light yield for x rays in the keV region drops to approximately equal to half of the one in the MeV region. A few percent of variations of light yields measured among different crystals is possibly due to the different Y and Ce concentrations [29]. This nonproportionality effect is due to the scintillation quenching caused by the high ionization density of the relatively slow electrons produced in the low-energy x-ray conversion. A recent

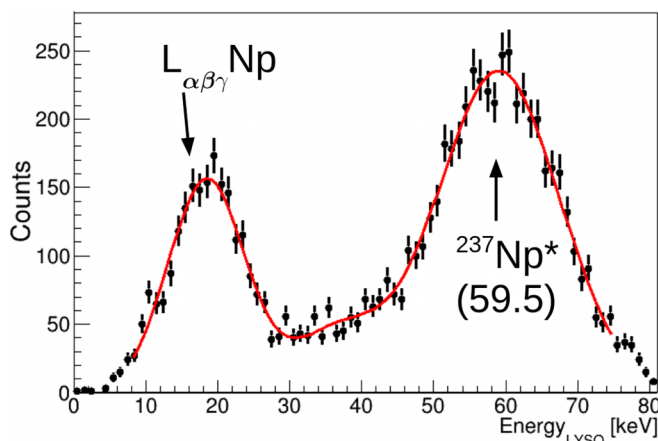


FIG. 5. LYSO scintillator energy spectrum for the  $^{241}\text{Am}$  calibration source. The red line is a multi-Gaussian fit considering the 59.5-keV peak from the  $^{237}\text{Np}^*$  decay and the folded contribution of  $L_{\alpha\beta\gamma}$  Np x rays to measure the detector's energy resolution.

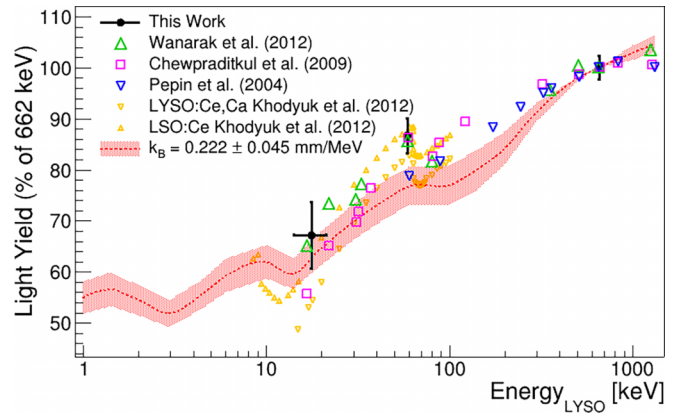


FIG. 6. The light yield measured for our LYSO crystal (black points) is compared with the existing published measurements for other similar crystals [26–29]. The red line is the result of a GEANT4 simulation of the expected light yield using the quenching parameters of Ref. [30] and varying  $k_B$  within the measurement uncertainty (red line and red area).

measurement of Birks-Osager quenching parameters for the LYSO scintillator used a 30 GeV/n argon beam (and nuclear fragments) [30]. There the luminous efficiency of LYSO was modeled as

$$L_{\text{eff}} = (1 - \eta_e/h e^{-k_o \frac{dE}{dx}}) \left( \frac{1 - \eta_H}{1 + (1 - \eta_H)k_B \frac{dE}{dx}} + \eta_H \right),$$

where the first factor describes the Onsager mechanism while the second one accounts for the (modified) Birks' law [30]. In Fig. 6 the light yield measured for our LYSO crystal (black points) is compared with the existing published measurements for other similar crystals [26–29]. A GEANT4 [31] simulation of the expected light yield using the quenching parameters of Ref. [30] is also shown for comparison (red line). In this work the energy scale of our LYSO scintillator has been evaluated taking into account the light yield nonproportionality expected from this simulation, we check that different modeling of the light yield nonproportionality has a small or negligible impact on the results.

The measured energy resolution of the LYSO scintillator is shown in Fig. 7. It is important to note that for the LYSO scintillator, an intrinsic energy resolution,  $\sigma_I$ , exists. This is due to the different processes involved in the  $\gamma$ -ray conversion providing electrons of different energies (thus differently quenched). The intrinsic resolution evaluated by a GEANT4 simulation using the quenching parameters of Ref. [30] is also shown in Fig. 7 and compared with the LYSO intrinsic resolution measured by Refs. [27,28]. The energy resolution of our LYSO scintillator was modeled as  $\sigma_{\text{LYSO}} = \sqrt{\sigma_0^2 + E/n^* + \sigma_I^2}$ , where  $\sigma_0 \simeq 1$  keV is the electronic noise contribution (the LYSO pedestal was measured with  $^{241}\text{Am}$  source on the HPGe),  $n^* = 1.8 \pm 0.5$  photoelectrons/keV is the number of collected photoelectrons for detected energy unity and  $\sigma_I$  is the expected intrinsic resolution for the LYSO.

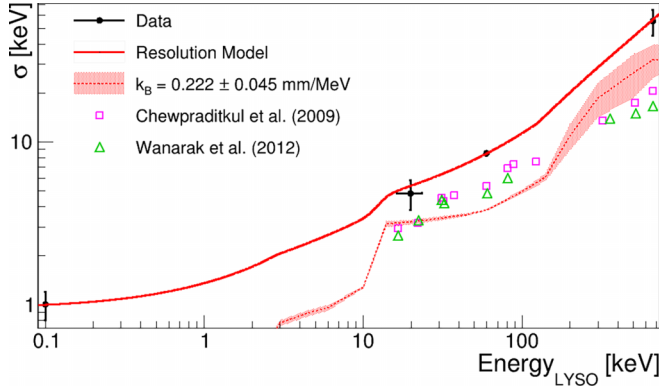


FIG. 7. Measured energy resolution for the LYSO scintillator (black points). The red dashed line is the expected LYSO intrinsic energy resolution,  $\sigma_I$ , evaluated with a GEANT4 simulation using the quenching parameters of Ref. [30] and varying  $k_B$  within the measurement uncertainty (solid area). The intrinsic resolution published for a similar LYSO scintillator is shown for comparison (squares and triangles [27,28]). The red continuous line is the model of the energy resolution measured for our LYSO scintillator.

### III. SEARCH FOR $^{176}\text{Lu}$ EC

Most of the events collected by the HPGe detector come from the  $^{176}\text{Lu}$   $\beta$  decay and the intrinsic or environmental background. These two classes of events are well recognized in the bidimensional spectrum of Fig. 8. In particular, the population of events characterized by  $E_{\text{LYSO}} < 3$  keV (vertical strip in Fig. 8) are mostly due to the intrinsic or environmental background. On the other hand, events characterized by  $E_{\text{LYSO}} > 3$  keV are mostly due to the continuous electron distribution emitted by  $^{176}\text{Lu}$   $\beta$  decay. For this last class of events, in Fig. 8 are also visible the  $^{176}\text{Hf}^*$   $\gamma$  lines characterized by a fixed energy detected in the high-purity germanium detector (HPGe) detector and the relative continuous distributions due to the Compton scattering. Similarly, at lower energy, the Hf x rays due to internal conversion of  $^{176}\text{Hf}^*$  levels and the Lu x rays due to photoelectric absorption, within the crystal, of  $^{176}\text{Hf}^*$   $\gamma$  rays are visible.

The powerful background rejection provided by the active source technique can be noticed in Fig. 8. All the events with LYSO energy larger than 27 or 50 keV are rejected and the

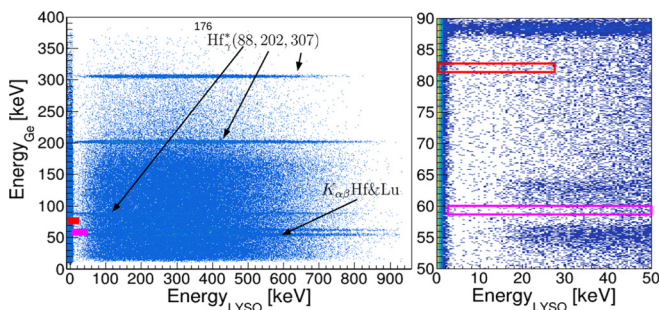


FIG. 8.  $E_{\text{Ge}}$  vs  $E_{\text{LYSO}}$  spectra and a zoom-in of the region of interest for EC. Red and magenta boxes are the region of interest for  $^{176}\text{Lu}$  EC to  $^{176}\text{Yb}^*$  and to ground states, respectively.

region of interest for the  $^{176}\text{Lu}$  EC decay to  $^{176}\text{Yb}$  excited state and ground state shrinks down to the red and magenta boxes. The measurement of the energy deposited in the LYSO allows us to tag (and reject) most of the background from the  $^{176}\text{Lu}$   $\beta$  decay.

#### A. Search for $^{176}\text{Lu}$ EC to $^{176}\text{Yb}^*$

Considering the fifth-forbidden EC transition of  $^{176}\text{Lu}$  to  $^{176}\text{Yb}^*$ , a strong identification signature is the 82.1-keV deexcitation  $\gamma$ -ray observed in the HPGe detector. The maximum neutrino energy for this decay is

$$E_{82}^{\nu\text{max}} = Q_{\text{EC}} - E_b - 82.1 \text{ keV},$$

where  $E_b$  is the Yb atomic binding energy of the captured electron [32], and therefore the capture of the  $1s$  electron is not energetically allowed for this detection channel.

In Fig. 9(a) the energy spectrum measured with our HPGe detector is shown (magenta line). These data are plotted without any requirement on the LYSO measured energy, and as a consequence, this plot is dominated by the background from the  $^{176}\text{Lu}$   $\beta$  decay. This corresponds to the typical landscape of the passive source measurement approach used in Ref. [5].

Profiting from the “active source” technique, most of  $^{176}\text{Lu}$   $\beta$ -decay events are rejected by the request  $E_{\text{LYSO}} < 27$  keV, i.e., the maximum expected energy in LYSO for the EC [blue points in Fig. 9(a)].

This approach provides a factor  $\approx 20$  in background suppression, and the resulting measured spectrum mostly corresponds to the intrinsic or environmental background characteristic of our HPGe detector. The black points in Fig. 9(a) are indeed our measurement of such background already shown in Fig. 3. The other relevant feature is the 88.3-keV peak from the  $^{176}\text{Hf}^*$  last deexcitation, which becomes evident observing the residuals after the HPGe background subtraction [see Fig. 9(b)].  $N_{82} = 38 \pm 105$  events are obtained by fitting the residuals, and thus no statistical evidence for the  $^{176}\text{Yb}^*$  82.1-keV peak was found. The corresponding 95% C.L. upper limit for a  $^{176}\text{Lu}$  EC process is estimated to be 210 events [dotted line in Fig. 9(b)].

Following the approach of Ref. [5] the upper limit on the EC branching fraction can be obtained by comparing the upper limit on the number of the  $^{176}\text{Yb}^*$  82.1-keV deexcitation  $\gamma$  rays with the number of  $^{176}\text{Hf}^*$  events measured by fitting the 88.3-keV  $\gamma$  line in the whole event distribution and thus related to the  $\beta$ -decay branching fraction ( $N_{88} = 119.9 \pm 0.5 \times 10^3$  events):

$$B_{82} = \frac{(1 + \alpha_T^{82})N_{82}/\varepsilon_{88}}{(1 + \alpha_T^{88})N_{88}} < 2.6 \times 10^{-3} \text{ (95\% C.L.)}, \quad (1)$$

where  $\alpha_T^{82} = 7.06$  and  $\alpha_T^{88} = 5.86$  are the total electron conversion coefficients for first excited levels of  $^{176}\text{Yb}$  and  $^{176}\text{Hf}$ , respectively [10,25], and  $\varepsilon_{88}(82) \simeq 80\%$  is the detection efficiency loss of the 82-keV  $\gamma$ -ray with respect to the 88-keV  $\gamma$ -ray.

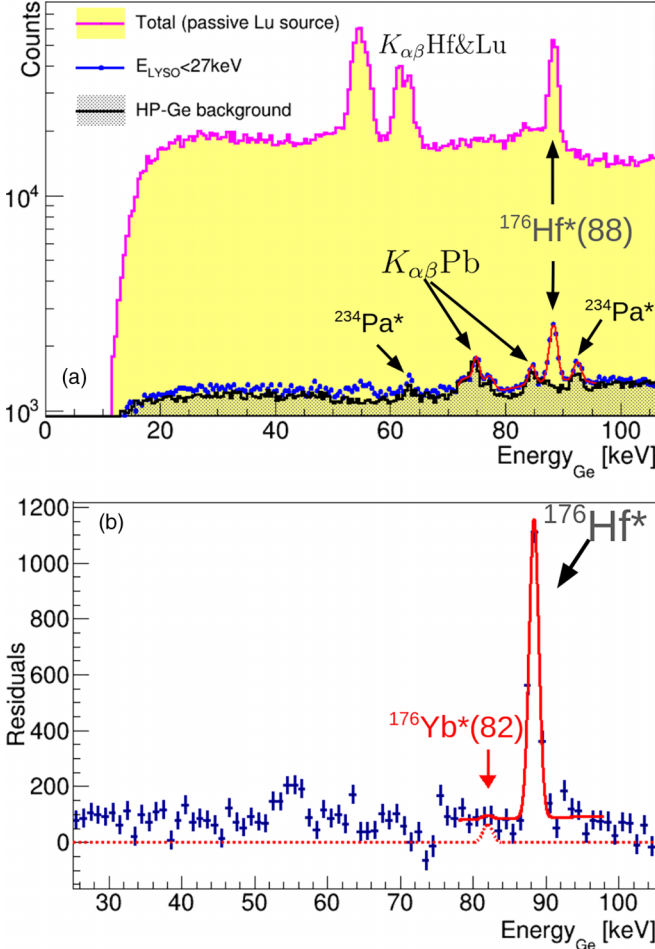


FIG. 9. Search for the  $^{176}\text{Yb}^*$  82.1-keV deexcitation  $\gamma$  ray. The cut  $E_{\text{LYSO}} < 27$  keV allows a background reduction of a factor  $\approx 20$  with respect to the “passive source” approach. The red arrow points out the expected position for the  $^{176}\text{Yb}^*$  82.1-keV peak in the background-subtracted residual spectrum. The red continuous line is a model considering Gaussian peaks over a flat background, and the red dashed line is the 95% upper limit for the 82.1-keV peak contribution.

### B. Search for REC or specific EC channels

The result presented in the previous section represents a cautious upper limit that holds for all possible channels of EC of  $^{176}\text{Lu}$  to  $^{176}\text{Yb}^*$ . However, with our setup, a specific energy distribution is expected to be observed with the LYSO crystal, for each kind of EC process. In particular, depending on the specific (sub)shell of the captured Lu electron, the relative binding energy is released in the LYSO crystal as a consequence of the Yb atomic rearrangement, emitting low-energy x rays or Auger electrons.

Figure 10 reports the expected energy releases in the LYSO crystal from  $L$ -shell,  $M$ -shell, and  $N$ -shell electron captures. These distributions are compared with the measured energy distribution in the LYSO scintillator for those events where the energy detected in the HPGe detector is  $82 \pm 2$  keV (shaded area). The measured signal is characterized by a peak at  $E_{\text{LYSO}} = 0$ , due to the intrinsic or environmental background,

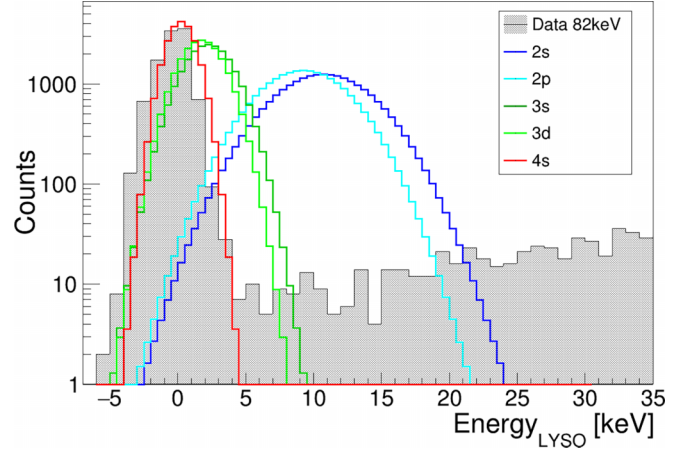


FIG. 10. Expected energy distributions in the LYSO crystal due to  $L$ -shell,  $M$ -shell, and  $N$ -shell electron captures. The shaded energy distribution is the measured one by selecting  $82 \pm 2$  keV energy deposited in the HPGe detector.

and by a continuous distribution due to the electron energy emitted by the  $^{176}\text{Lu}$   $\beta$  decay.

On the other hand, in the case of a REC, also the low-energy x-ray emitted is detected in the LYSO crystal together with the electron binding energy. Following the formalism of Ref. [33], the x-ray energy distribution expected for a REC is

$$\frac{dN_x(k)}{dk} = N_0 R_x(k) k \left(1 - \frac{k}{q_x}\right)^2, \quad (2)$$

where  $k$  is the x-ray energy,  $x$  denotes the considered atomic electron,  $q_x$  is the maximum allowed x-ray energy in the REC,  $R_x(k)$  is a model-dependent shape factor, and  $N_0$  is an overall normalization.

For the internal bremsstrahlung of  $s$ -state electrons (characterized by a larger wave-function overlap with the nucleus) an analytic model for  $R_{\text{ns}}$  can be produced following some reasonable approximations [33]. However, the general analytical form for the shape factor of REC of  $ns$ -level electrons can be expressed as [20]

$$R_x(k) = A_x^{(1)} \left(1 - \frac{k}{q_x}\right)^2 + A_x^{(2)} \Lambda \left(\frac{k}{q_x}\right)^2 + 2 \left(\frac{e_{\text{eff}} m_e}{q_x}\right)^2 + A_x^{(3)} e_{\text{eff}} \frac{m_e k}{q_x^2}, \quad (3)$$

where  $A_x^{(i)}(k) \approx 1$  are describing Coulomb effects,  $\Lambda$  represents a combination of reduced nuclear matrix elements, and the last two terms arise from the possible contribution due to detour transitions (DT). In the latter case, the parameter  $e_{\text{eff}}$ , the effective charge, represents the strength of the DT. Entering into the details of a model of the possible REC for  $^{176}\text{Lu}$  is beyond the purpose of this work; however, it is interesting to note that for the case of the measured REC of heavy nuclei, like  $^{137}\text{La}$  and  $^{204}\text{Tl}$ , the contribution of detour transitions appears to be negligible [20,21]. Moreover, we also verify that the variation of  $\Lambda$  from 0 to 1 introduces only

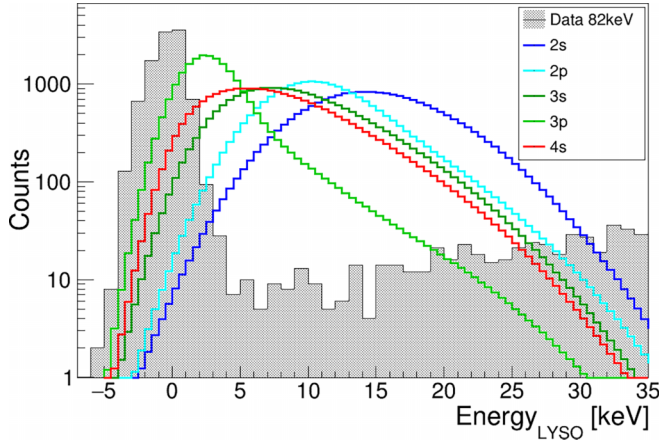


FIG. 11. Expected energy distributions in the LYSO crystal due to radiative electron captures. The shaded energy distribution is the measured one by selecting  $82 \pm 2$  keV energy deposited in the HPGe detector.

small modifications (within 10%) of our results. We fix, for simplicity,  $\Lambda = 0$  and  $e_{\text{eff}} = 0$ , thus assuming the minimal contribution of REC x-ray energy in the LYSO spectrum. Regarding REC from  $2p$  and  $3p$  shells we derive the shape factors from the numerical tables in Ref. [33]. In Fig. 11 the energy distributions expected in the LYSO scintillator for some REC channels are shown.

The analysis proceeds by searching for the 82.1-keV peak in the HPGe energy distributions considering two different selections for  $E_{\text{LYSO}}$  and evaluating the relative signal efficiency from the expected energy distributions of Figs. 10 and 11. The selections on  $E_{\text{LYSO}}$  will improve the overall signal-over-background ratio. In Fig. 12 the HPGe energy distribution considering the selection  $2 \text{ keV} < E_{\text{LYSO}} < 20 \text{ keV}$  is shown;

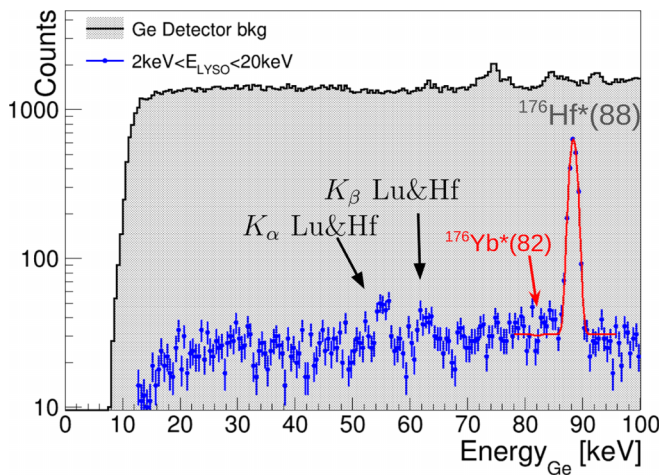


FIG. 12. Search for  $L$ -shell EC or REC or for  $ns$ -shell REC of  $^{176}\text{Lu}$  in the  $^{176}\text{Yb}^*$  82.1-keV level. The cut  $2 \text{ keV} < E_{\text{LYSO}} < 20 \text{ keV}$  allows further background reduction of a factor  $\approx 40$  with respect to the intrinsic or external detector background (shaded). The red line is a fit model considering the 88.3-keV  $^{176}\text{Hf}^*$  and the possible 82.1-keV  $^{176}\text{Yb}^*$  peaks over a flat background.

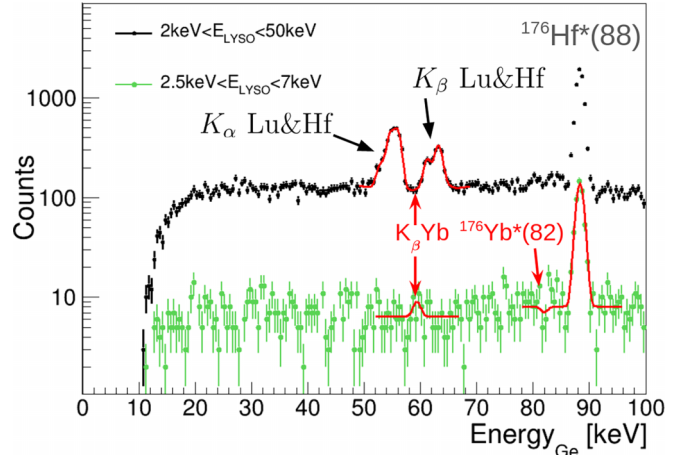


FIG. 13. Search for EC and REC of  $^{176}\text{Lu}$  in the  $^{176}\text{Yb}^*$  82.1-keV level and in the  $^{176}\text{Yb}$  fundamental state. The selection  $2.5 \text{ keV} < E_{\text{LYSO}} < 7 \text{ keV}$  allows us to search for  $K$ -shell EC ( $K_{\beta} = 59.3\text{-keV}$  x ray) or  $M$ - and  $N$ -shell EC and REC to the 82.1-keV level. The red lines are the fit models to investigate the possible presence of the Yb 59.3-keV  $K_{\beta}$  or the  $^{176}\text{Yb}^*$  82.1-keV peaks considering the contribution of the other  $\gamma$ -ray and x-ray Gaussian peaks over a continuous background.

this allows the rejection of most of the intrinsic detector background, providing a further  $\approx 40$  reduction factor with respect to the counting rate shown in Fig. 9.

The number of events that can be attributed to  $^{176}\text{Yb}^*$  is  $N_{82} = -2 \pm 12$ , and thus no statistical evidence for the EC or REC is found in this energy window. Considering the slightly different  $E_{\text{LYSO}}$  selection efficiencies for the different subchannels (98% to 82%), the limits to the branching ratio,  $< 0.024\%$  and  $\lesssim 0.028\%$  at 95% C.L., can be inferred for the  $L$ -shell EC and  $ns$  REC, respectively. Limits on these channels are relative to electrons whose wave functions are more overlapped with the nucleus, and they are more than 1 order of magnitude lower when compared with previous ones based on the passive lutetium source [5].

On the other hand, Fig. 13 shows the measured events in the  $2.5 \text{ keV} < E_{\text{LYSO}} < 7 \text{ keV}$  energy window; this is suitable for the study of the  $M$ - and  $N$ -shell REC channels or the  $M$ -shell EC channel releasing a smaller energy contribution within the LYSO crystal. In this case the number of events that can be attributed to  $^{176}\text{Yb}^*$  is  $N_{82} = -3 \pm 6$ , and thus the upper limit to  $N_{82}$  is more stringent; however, the selection efficiency for these channels is relatively small (in the 30%–45% range). Table I summarizes the branching ratio limits obtained in the different subchannels.

Finally, the precise shape factors for REC of  $d$  and  $f$  electron orbitals are not quantitatively evaluated in the literature; however, it is reasonable to expect a very soft internal bremsstrahlung spectrum for  $4f$  electron REC, providing a negligible energy deposition within the LYSO scintillator. It is important to note that REC of  $4f$  electrons in  $^{176}\text{Lu}$  is a very interesting channel since it allows a neutrino emission with  $\hbar/2$  total angular momentum. A dedicated investigation of the region  $E_{\text{LYSO}} < 4 \text{ keV}$  provides the largest excess,

TABLE I. Upper limits on the branching fraction for specific electron capture channels of  $^{176}\text{Lu}$ .

Electron capture channel	Branching ratio limit (95% C.L.)	Previous limit (68% C.L.) [5]
1s EC + 59 keV	0.035%	0.36%
1s REC + 59 keV	0.029%	
$L$ EC + 82 keV	0.024%	0.45%
$L/3s$ REC + 82 keV	0.026%	
$n_{>3s}$ REC + 82 keV	0.028%	
$3p$ REC + 82 keV	0.036%	
$3s/3p$ EC + 82 keV	0.027%	
$3d$ EC + 82 keV	0.038%	
Any + 82 keV	0.26%	

$N_{82} = 167 \pm 100$ , observed in this experiment; however, this is still fully compatible with the expected statistical fluctuations.

### C. Search for $^{176}\text{Lu}$ $K$ -shell EC and REC

The EC decay of  $^{176}\text{Lu}$  to the fundamental state of  $^{176}\text{Yb}$  is a seventh-degree forbidden transition; thus, it is expected to be suppressed with respect to the fifth-degree forbidden EC decay in  $^{176}\text{Yb}^*$ . However, if a  $^{176}\text{Lu}$  nucleus captures a  $K$ -shell electron, the result must be a  $^{176}\text{Yb}$  nucleus in the ground state. Considering that the  $K$ -shell atomic orbital is the one with the largest superposition with the nucleus, this possibility deserves a dedicated investigation.

A signature of the  $K$ -shell capture is provided by the x rays emitted when the Yb atomic vacancy is filled. In particular,  $K_{\alpha 2} = 51.35$  keV,  $K_{\alpha 1} = 52.4$  keV, and  $K_{\beta} = 59.3$  keV are emitted with a probability of 27.2%, 48.1%, and 15.1%, respectively [1]. By comparing these x-ray energies with the measured energy distribution (see, e.g., Fig. 13), it is clear that the Yb  $K_{\beta}$  line is the only one distant enough from the nearby Lu and Hf  $K$ -shell lines to be easily identified. Moreover, due to self-absorption in the LYSO crystal and in the HPGe dead layers, the expected detection efficiency for Yb  $K_{\alpha}$  lines is quite small, whereas the Yb  $K_{\beta}$  line has  $\varepsilon_{88} \simeq 100\%$  (see Fig. 4).

To search the Yb  $K_{\beta}$  line, we must first recall that the  $Q$  value for  $^{176}\text{Lu}$  EC is  $\simeq 109$  keV, and if the emitted x-ray accounts for 59.3 keV, the maximum energy that we might detect in the LYSO crystal is  $\simeq 50$  keV. This value, however, represents only the end point of the possible REC energy distribution. On the other hand, knowing that the  $K$ -shell ionization energy in Yb is 61.3 keV, it is possible to estimate a minimum energy of 2 keV detected in the LYSO from the additional x rays and Auger electrons emitted by the Yb atomic deexcitation.

Assuming the detection of Yb  $K_{\beta}$  x-ray in the HPGe detector, in Fig. 14, we show the REC energy distribution (magenta) and the 2-keV contribution folded with the LYSO energy resolution (green). In Fig. 14, the expected EC signal distributions are compared with the measured LYSO energy distribution for the events where a 59-keV signal is observed in the HPGe detector (shaded area). Sim-

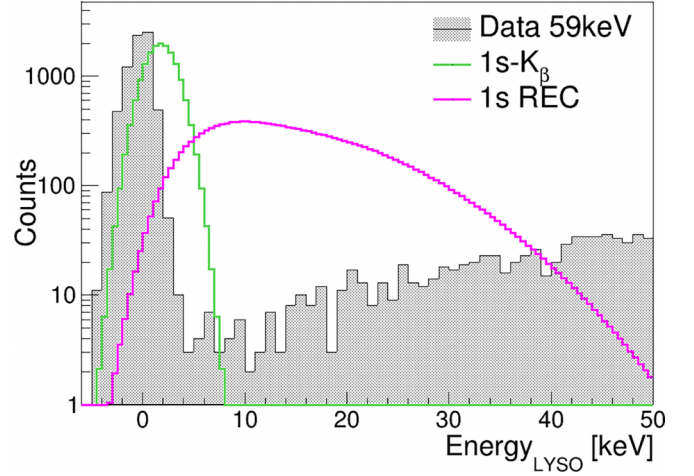


FIG. 14. Expected LYSO energy distributions for EC (green line) and REC (magenta line) of  $^{176}\text{Lu}$  in the  $^{176}\text{Yb}$  ground state. As a comparison the LYSO energy distribution for 59.3 keV measured in the HPGe detector is shown (shaded area).

ilarly to Figs. 10 and 11, also this measured distribution is characterized by a peak at  $E_{\text{LYSO}} = 0$  due to intrinsic or external HPGe background and a continuous distribution due to the known  $^{176}\text{Lu}$   $\beta$  decay.

The measured HPGe energy distribution obtained when applying the selection  $2 \text{ keV} < E_{\text{LYSO}} < 50 \text{ keV}$  is shown in Fig. 13. In this plot the number of events attributed to a possible Yb  $K_{\beta}$  peak is  $N_{59} = 3 \pm 42$ , and thus no evidence for REC capture of  $K$ -shell electrons is found. The upper limit to the corresponding branching fraction is

$$B_{59} = \frac{N_{59}/(\varepsilon_{59}\varepsilon_{88}\varepsilon_{\text{sel}})}{(1 + \alpha_T^{88})N_{88}} < 6 \times 10^{-4} \text{ (95\% C.L.)}, \quad (4)$$

where  $\varepsilon_{59} = 15.1\%$  is the probability of a  $K_{\beta}$  x-ray emission filling an Yb  $K$ -shell vacancy,  $\varepsilon_{88} \simeq 100\%$  is the detection efficiency of a 59-keV  $\gamma$  ray with respect to an 88-keV  $\gamma$  ray, and  $\varepsilon_{\text{sel}} \simeq 98\%$  is the efficiency for the expected REC distribution considering the  $2 \text{ keV} < E_{\text{LYSO}} < 50 \text{ keV}$  selection.

By restricting the LYSO window to the 2–20 keV range ( $\varepsilon_{\text{sel}} \simeq 70\%$ ), the  $\beta$ -decay background was reduced by a factor  $\approx 5$ , and we found  $N_{59} = -2 \pm 15$ ; thus, the upper limits to the REC branching fraction improved to  $B_{59} < 2.9 \times 10^{-4}$  (95% C.L.).

The pure  $K$ -shell EC (green line in Fig. 14) was investigated by considering the  $2.5 \text{ keV} < E_{\text{LYSO}} < 7 \text{ keV}$  selection ( $\varepsilon_{\text{sel}} \simeq 30\%$ ), and the number of events attributed to a possible Yb  $K_{\beta}$  peak are  $N_{59} = 4 \pm 6$ . Thus, also for this process, no evidence is found and the upper limit is  $B_{59} < 3.5 \times 10^{-4}$  (95% C.L.).

## IV. DISCUSSION AND CONCLUSIONS

The search for electron capture in  $^{176}\text{Lu}$  is an opportunity for a laboratory measurement of fifth-degree forbidden processes that may provide valuable information for nuclear theory models. Our active source technique, which uses a LYSO crystal scintillator also as a detector, allows a

powerful reduction of the background from  $^{176}\text{Lu}$   $\beta$  decay and the HPGe intrinsic or external contamination. No evidence for the EC process was found. Depending on the particular EC channel, we were able to set upper limits for the  $^{176}\text{Lu}$  EC branching fraction that are a factor of 3–30 better than what was obtained with previous measurements [5]. Table I reports our estimation of the upper limits for the different EC channels.

Considering the known  $\approx 38$ -Gyr half-life of  $^{176}\text{Lu}$ , the obtained limits on the partial half-life for the EC processes are in the range of a few  $\times 10^{13}$ – $10^{14}$  y. It is interesting to compare these limits with the partial half-life of the other five naturally occurring isotopes that can decay via the EC process:

$$^{40}\text{K}(4^-) \rightarrow ^{40}\text{Ar}(2^+)T_{1/2}^{\text{EC}} = 1.2 \times 10^{10} \text{ y [1]},$$

$$^{50}\text{V}(6^+) \rightarrow ^{50}\text{Ti}(2^+)T_{1/2}^{\text{EC}} = 2.7 \times 10^{17} \text{ y [2,3]},$$

$$^{138}\text{La}(5^+) \rightarrow ^{138}\text{Ba}(2^+)T_{1/2}^{\text{EC}} = 1.6 \times 10^{11} \text{ y [1]},$$

$$^{123}\text{Te}(1/2^+) \rightarrow ^{123}\text{Sb}(7/2^+)T_{1/2}^{\text{EC}} > 3 \times 10^{16} \text{ y [4]},$$

$$^{180m}\text{Ta}(9^-) \rightarrow ^{180}\text{Hf}(6^+)T_{1/2}^{\text{EC}} > 2 \times 10^{17} \text{ y [6]}.$$

This comparison suggests that improvements in sensitivity of 2–3 orders of magnitude could be possible, in principle, by

adopting the techniques of low-background experiments. In particular, moving to the HPGe facility of an underground laboratory the intrinsic or external background would be reduced by a few orders of magnitude. Moving to an underground laboratory would be important also to suppress the tricky background due to the possible environmental neutron capture of the (97.4%) abundant  $^{175}\text{Lu}$  isotope that could produce the  $^{176m}\text{Lu}$  ( $1^-$ ) 123-keV level. It is known that this nuclear isomer, whose half-life is 3.6 h, undergoes EC populating both the ground state and the ( $2^+$ ) levels of  $^{176}\text{Yb}$  [10]. Finally, both the HPGe and LYSO energy resolutions can be improved. In particular by considering the possibility to operate small LYSO crystals as cryogenic bolometers, a very good signature of EC peaks in the LYSO spectrum is expected.

## ACKNOWLEDGMENTS

We thank the student G. Bertuolo who collaborated with us on the measurements on the first LYSO detector prototypes. Moreover, we are grateful to our UniTN Laboratory colleagues: M. Hueller, M. T. López-Arias Montenegro, P. Minati, and M. Di Mauro, for their support with regard to the HP-Ge operations.

- 
- [1] S. Chu, L. Ekström, and R. Firestone, Table of radioactive isotopes, database version 1999-02-28, <http://nucleardata.nuclear.lu.se/toi/>.
- [2] M. Laubenstein, B. Lehnert, S. S. Nagorny, S. Nisi, and K. Zuber, New investigation of half-lives for the decay modes of  $^{50}\text{V}$ , *Phys. Rev. C* **99**, 045501 (2019).
- [3] F. A. Danevich, M. Hult, D. V. Kasperovych, V. R. Klavdiienko, G. Lutter, G. Marissens, O. G. Polischuk, and V. I. Tretyak, Decay scheme of  $^{50}\text{V}$ , *Phys. Rev. C* **102**, 024319 (2020).
- [4] D. Münstermann and K. Zuber, An alternative search for the electron capture of  $^{123}\text{Te}$ , *J. Phys. G: Nucl. Part. Phys.* **29**, B1 (2003).
- [5] E. Norman, E. Browne, I. Goldman, and P. Renne, Improved limit on the electron capture decay branch of  $^{176}\text{Lu}$ , *Appl. Radiat. Isot.* **60**, 767 (2004).
- [6] B. Lehnert, M. Hult, G. Lutter, and K. Zuber, Search for the decay of nature's rarest isotope  $^{180m}\text{Ta}$ , *Phys. Rev. C* **95**, 044306 (2017).
- [7] K. Kossert, G. Jörg, and C. L. v. Gostomski, Experimental half-life determination of  $^{176}\text{Lu}$ , *Appl. Radiat. Isot.* **81**, 140 (2013), 6th International Conference on Radionuclide Metrology—Low Level Radioactivity Measurement Techniques.
- [8] M. Hult, T. Vidmar, U. Rosengård, G. Marissens, G. Lutter, and N. Sahin, Half-life measurements of lutetium-176 using underground HPGe-detectors, *Appl. Radiat. Isot.* **87**, 112 (2014), in *Proceedings of the 19th International Conference on Radionuclide Metrology and its Applications 17–21 June 2013*, Antwerp, Belgium.
- [9] J. R. de Laeter and N. Bukilic, Solar abundance of  $^{176}\text{Lu}$  and s-process nucleosynthesis, *Phys. Rev. C* **73**, 045806 (2006).
- [10] IAEA, Nuclear data <https://www-nds.iaea.org>, 2022
- [11] BNL,  $Q$ -value calculator (qcalc), <https://www.nndc.bnl.gov/qcalc/>, 2023.
- [12] W. Huang, M. Wang, F. Kondev, G. Audi, and S. Naimi, The AME 2020 atomic mass evaluation (I). Evaluation of input data, and adjustment procedures, *Chin. Phys. C* **45**, 030002 (2021).
- [13] M. Wang, W. Huang, F. Kondev, G. Audi, and S. Naimi, The AME 2020 atomic mass evaluation (II). Tables, graphs and references, *Chin. Phys. C* **45**, 030003 (2021).
- [14] B. Singh, J. Rodriguez, S. Wong, and J. Tuli, Review of  $\log ft$  values in  $\beta$  decay, *Nucl. Data Sheets* **84**, 487 (1998).
- [15] Saint-Gobain, LYSO, <https://www.crystals.saint-gobain.com/radiation-detection-scintillators/crystal-scintillators/lyso-scintillation-crystals>.
- [16] L. Kalinowski, Z. Janas, M. Pfützner, A. Płochocki, P. Hornshøj, and H. Nielsen, Detour transitions in forbidden radiative electron capture decay, *Nucl. Phys. A* **537**, 1 (1992).
- [17] B. Mysłek, Z. Sujkowski, and J. Żylicz, Internal bremsstrahlung in the unique first-forbidden electron capture decay of  $^{41}\text{Ca}$ , *Nucl. Phys. A* **215**, 79 (1973).
- [18] Z. Janas, M. Pfützner, A. Płochocki, P. Hornshøj, and H. Nielsen, Study of the internal bremsstrahlung accompanying the ( $2\nu$ )-forbidden electron capture decay of  $^{59}\text{Ni}$ , *Nucl. Phys. A* **524**, 391 (1991).
- [19] S. Mianowski, E. Werner-Malento, A. Korgul, M. Pomorski, K. Pachucki, M. Pfützner, B. Szeweryn, J. Żylicz, P. Hornshøj, T. Nilsson, and K. Rykaczewski, Radiative electron capture in the first-forbidden unique decay of  $^{81}\text{Kr}$ , *Phys. Rev. C* **82**, 044308 (2010).
- [20] M. Pfützner, P. Hornshøj, H. Nielsen, J. Kurpeta, and A. Płochocki, Radiative electron capture in the second forbidden decay of  $^{137}\text{La}$ , *Nucl. Phys. A* **611**, 270 (1996).
- [21] J. Kurcewicz, M. Pfützner, P. Hornshøj, H. Nielsen, and B. Szeweryn, Radiative electron capture in the first forbidden unique decay of  $^{204}\text{Tl}$ , *Nucl. Phys. A* **728**, 3 (2003).



- [22] Mirion, Standard electrode coaxial Ge detectors, <https://www.mirion.com/products/sege-standard-electrode-coaxial-ge-detectors>.
- [23] LeCroy, <https://teledynelecroy.com/oscilloscope/waverunner-9000-oscilloscopes/waverunner-9104>.
- [24] B. Mauz, P. J. Nolan, and P. G. Appleby, Technical note: Quantifying uranium-series disequilibrium in natural samples for dosimetric dating—Part 1: gamma spectrometry, *Geochronology* **4**, 213 (2022).
- [25] T. Kibédi, Jr., T. Burrows, M. Trzhaskovskaya, P. Davidson, and C. Nestor, Evaluation of theoretical conversion coefficients using BrIcc, *Nucl. Instrum. Methods Phys. Res., Sect. A* **589**, 202 (2008).
- [26] C. Pepin, P. Berard, A.-L. Perrot, C. Pepin, D. Houde, R. Lecomte, C. Melcher, and H. Dautet, Properties of LYSO and recent LSO scintillators for phoswich PET detectors, *IEEE Trans. Nucl. Sci.* **51**, 789 (2004).
- [27] W. Chewpraditkul, L. Swiderski, M. Moszynski, T. Szczesniak, A. Syntfeld-Kazuch, C. Wanarak, and P. Limsuwan, Scintillation properties of LuAG:Ce, YAG:Ce and LYSO:Ce crystals for gamma-ray detection, *IEEE Trans. Nucl. Sci.* **56**, 3800 (2009).
- [28] C. Wanarak, W. Chewpraditkul, and A. Phunpueok, Light yield non-proportionality and energy resolution of  $\text{Lu}_{1.95}\text{Y}_{0.05}\text{SiO}_5:\text{Ce}$  and  $\text{Lu}_2\text{SiO}_5:\text{Ce}$  scintillation crystals, *Procedia Eng.* **32**, 765 (2012).
- [29] I. V. Khodyuk and P. Dorenbos, Trends and patterns of scintillator nonproportionality, *IEEE Trans. Nucl. Sci.* **59**, 3320 (2012).
- [30] O. Adriani *et al.*, Light yield non-proportionality of inorganic crystals and its effect on cosmic-ray measurements, *J. Instrum.* **17**, P08014 (2022).
- [31] J. Allison, K. Amako, J. Apostolakis, P. Arce, M. Asai, T. Aso, E. Bagli, A. Bagulya, S. Banerjee, G. Barrand *et al.*, Recent developments in GEANT4, *Nucl. Instrum. Methods Phys. Res., Sect. A* **835**, 186 (2016).
- [32] J. A. Bearden and A. F. Burr, Reevaluation of x-ray atomic energy levels, *Rev. Mod. Phys.* **39**, 125 (1967).
- [33] R. J. Glauber and P. C. Martin, Radiative capture of orbital electrons, *Phys. Rev.* **104**, 158 (1956).